JOURNAL OF CATALYSIS **159,** 170–177 (1996)
ARTICLE NO. 0076

Characterization of Vanadium Oxide–Zirconia Catalyst

Jong Rack Sohn,*,[1] Sung Guk Cho,* Young Il Pae,† and Shigenobu Hayashi‡

*Department of Industrial Chemistry, Engineering College, Kyungpook National University, Taegu 702-701, Korea; †Department of Chemistry, University of Ulsan, Ulsan 680-749, Korea; and ‡National Institute of Materials and Chemical Research, Tsukuba, Ibaraki 305, Japan

Received March 8, 1995; revised September 29, 1995; accepted November 22, 1995

Vanadium oxide–zirconia catalysts were prepared by dry impregnation of powdered $Zr(OH)_4$ with an aqueous solution of NH_4VO_3. The surface characterization of prepared catalysts was performed using FTIR, DSC, ^{51}V solid state NMR, and XRD, and by the measurement of surface area. The addition of vanadium oxide up to 9 mol% to zirconia shifted the phase transitions of ZrO_2 from amorphous to tetragonal toward higher temperatures due to the interaction between vanadium oxide and zirconia. On the basis of results of IR, XRD, and DSC, it is concluded that the content of V_2O_5 monolayer covering most of the available zirconia is 9 mol%, giving 2.3 V_2O_5 molecules/nm^2. Since the ZrO_2 dispersed vanadium oxide, the crystalline V_2O_5 was observed only with the samples containing V_2O_5 content exceeding the formation of complete monolayer (9 mol%) on the surface of ZrO_2. For the samples calcined at 673 K the acidity and surface area increase abruptly upon the addition of 0.2 mol% V_2O_5 to ZrO_2, and then both of them increase with increasing V_2O_5 content up to 5 mol%, showing the presence of Brønsted and Lewis acid sites on the V_2O_5/ZrO_2 catalyst. © 1996 Academic Press, Inc.

INTRODUCTION

Supported metal oxides exhibit interesting catalytic behavior depending on the kind of support, the content of active component, and the preparation method (1, 2). In particular, vanadium oxide catalysts in combination with various promoters are widely used for several reactions including oxidation of hydrocarbons (3, 4), ammoxidation of aromatics and methylaromatics (5), and selective catalytic reduction of NO_x by NH_3 (6). These systems have also been found to be effective catalysts for the oxidation of methanol to methylformate (7, 8). Much research has been done to understand the nature of active sites and the surface structure of catalysts, as well as the role played by the promoter of the supported catalysts, using IR, XRD, E.S.R., and Raman spectroscopy (8–11). So far, however, they have been studied mainly on titania and alumina (12–15), and only a small amount of work was studied for the ZrO_2 support (16–18).

Zirconia is an important material due to its interesting thermal and mechanical properties and so has been investigated as a support and catalyst in recent years. Different papers have been devoted to the study of ZrO_2 catalytic activity in important reactions such as methanol and hydrocarbon synthesis from CO and H_2 or CO_2 and H_2 (19, 20) or alcohol dehydration (21, 22). Zirconia has been extensively used as a support for metals or incorporated in supports to stabilize them or make them more resistant to sintering (23–25). ZrO_2 activity and selectivity highly depend on the methods of preparation and the treatment used. In particular, in previous papers from this laboratory, it has been shown that NiO–ZrO_2 and ZrO_2 modified with sulfate ion, and CrO_x–ZrO_2 are very active for acid-catalyzed reactions (26–28). The high catalytic activities in the above reactions were attributed to the enhanced acidic properties of the modified catalysts, which originate from the inductive effect of S=O or Cr=O bonds of the complexes formed by the interaction of oxides with the sulfate or chromate ions.

It is well known that the dispersion and the structural features of supported species may strongly depend on the support. Structure and physicochemical properties of supported metal oxides are considered to be in different states compared with bulk metal oxides because of their interaction with supports. This paper describes the surface characterization of vanadium oxide supported on zirconia. The characterization of the samples was performed by means of Fourier transform infrared (FTIR), X-ray diffraction (XRD), solid state ^{51}V nuclear magnetic resonance (^{51}V NMR), differential scanning calorimetry (DSC), and measurement of surface area.

EXPERIMENTAL

Catalyst Preparation

The precipitate of $Zr(OH)_4$ was obtained by adding aqueous ammonia slowly into an aqueous solution of zirconium oxychloride at room temperature with stirring until the pH of mother liquor reached about 8. The precipitate thus obtained was washed thoroughly with distilled water until chloride ion was not detected, and was dried at room temperature for 12 h. The dried precipitate was powdered below 100 mesh.

[1] To whom correspondence should be addressed.

0021-9517/96 $18.00

The catalysts containing various vanadium oxide contents were prepared by dry impregnation of powdered $Zr(OH)_4$ with an aqueous solution of NH_4VO_3 followed by calcining at high temperature for 1.5 h in air. This series of catalysts is denoted by their mole percentage of V_2O_5. For example, 1-V_2O_5/ZrO_2 indicates the catalyst containing 1 mol% V_2O_5.

Characterization

FTIR absorption spectra of V_2O_5/ZrO_2 powders were measured by the KBr disk method over the range 1200–400 cm^{-1}. The samples for the KBr disk method were prepared by grinding a mixture of the catalyst and KBr powders in an agate mortar and pressing them in the usual way. FTIR spectra of pyridine adsorbed on the catalyst were obtained in a heatable gas cell at room temperature using a Mattson Model GL 6030E spectrophotometer. The self-supporting catalyst wafers contained about 9 mg/cm^2. Prior to obtaining the spectra the samples were heated under vacuum at 673 ~ 773 K for 1.5 h.

Catalysts were checked in order to determine the structure of the support as well as that of vanadium oxide by means of a Jeol Model JDX-8030 diffractometer, employing Cu$K\alpha$ (Ni-filtered) radiation.

^{51}V NMR spectra were measured by a Bruker MSL400 spectrometer with a static magnetic field strength of 9.4 T. Larmor frequency was 105.25 MHz. The ordinary single pulse sequence was used, in which the pulse width was set at 0.8 μs and the repetition time was 0.1 s. The $\pi/2$ pulse width adjusted for solution was 12 μs. The spectral width was 1.25 MHz. The number of scans was varied from 1000 to 12,000, depending on the concentration of vanadium. The signal was acquired from the time point 4 μs after the end of the pulse. The sample was static, and its temperature was ambient (294 K). The spectra were expressed with the signal of $VOCl_3$ being 0 ppm, and the higher frequency shift from the standard was positive. Practically, 0.16 *M* $NaVO_3$ aqueous solution (−574.28 ppm) was used as the second external reference (29).

DSC measurements were performed by a PL-STA model 1500H apparatus in air, and the heating rate was 5 K per minute. For each experiment 10–15 mg of sample was used.

The specific surface area was determined by applying the BET method to the adsorption of N_2 at 77 K. Chemisorption of ammonia was also employed as a measure of the acidity of catalysts. The amount of chemisorption was obtained as the irreversible adsorption of ammonia (30, 31).

RESULTS AND DISCUSSION

Infrared Spectra

Figure 1 shows infrared spectra of V_2O_5/ZrO_2 catalysts with various content calcined at 673 K for 1.5 h.

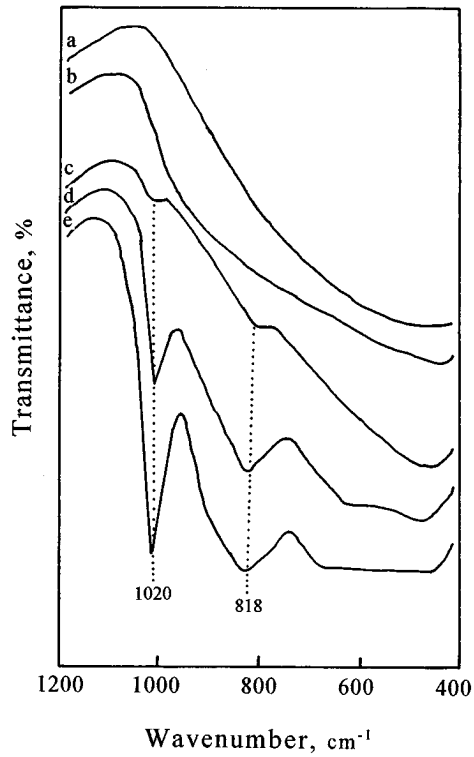

FIG. 1. Infrared spectra of (a) 5-V_2O_5/ZrO_2, (b) 9-V_2O_5/ZrO_2, (c) 15-V_2O_5/ZrO_2, (d) 20-V_2O_5/ZrO_2, and (e) V_2O_5.

Although with samples below 15 mol% of V_2O_5 the definite peaks were not observed, the absorption bands at 1020 and 818 cm^{-1} appeared for 15-V_2O_5–ZrO_2, 20-V_2O_5–ZrO_2, and pure V_2O_5 containing high V_2O_5 content. The band at 1020 cm^{-1} is assigned to the V=O stretching vibration, while that at 818 cm^{-1} is attributable to the coupled vibration between V=O and to V–O–V (32). Generally, the IR band of V=O in crystalline V_2O_5 shows at 1020–1025 cm^{-1} and the Raman band at 995 cm^{-1} (4, 33). As shown in Fig. 1, the catalysts at vanadia loadings below 15 mol% have no absorption bands due to crystalline V_2O_5.

Crystalline Structure of Catalyst

The crystalline structure of V_2O_5/ZrO_2 calcined in air at different temperatures for 1.5 h was examined. As shown in Fig. 2, ZrO_2 was amorphous to X-ray diffraction up to 573 K, with a two-phase mixture of the tetragonal and monoclinic forms at 623–873 K, and a monoclinic phase at 973 K. Three crystal structures of ZrO_2, tetragonal, monoclinic, and cubic phases, have been reported (34, 35).

However, in the case of supported vanadium oxide catalysts the crystalline structures of samples were different from that of support, ZrO_2. For the 2-V_2O_5/ZrO_2, as shown in Fig. 3, ZrO_2 was amorphous to X-ray diffraction up to 623 K. In other words, the transition temperature from amorphous to tetragonal phase was higher by 50 K than that

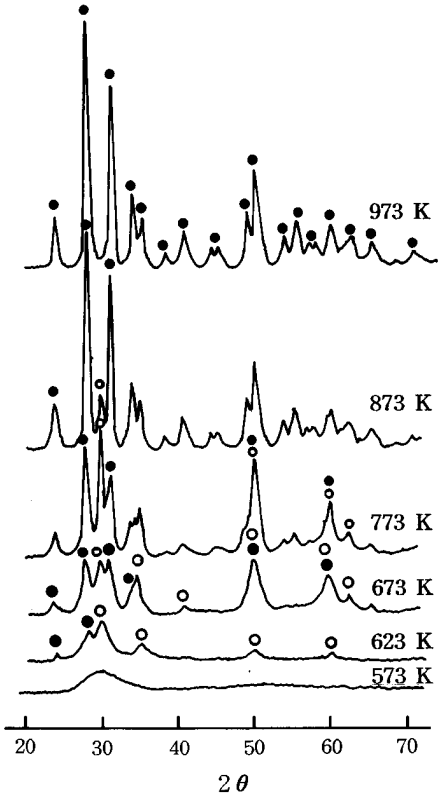

FIG. 2. X-ray diffraction patterns of ZrO_2 calcined at different temperatures for 1.5 h. ○, tetragonal phase ZrO_2; ●, monoclinic phase ZrO_2.

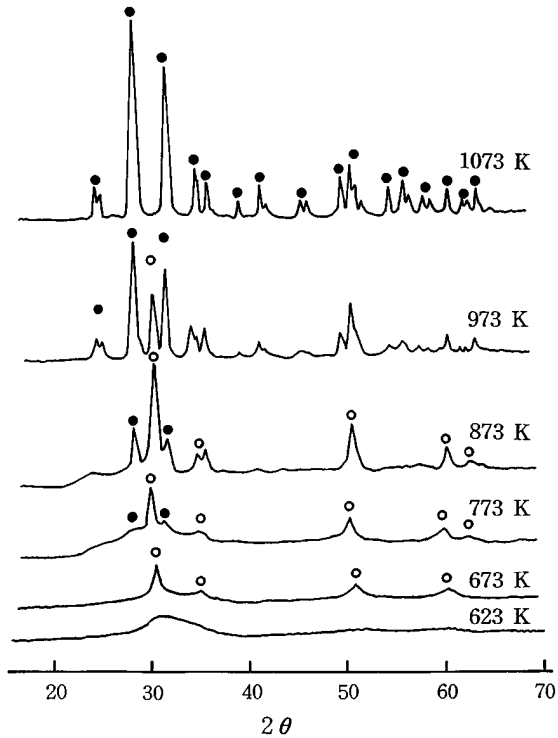

FIG. 3. X-ray diffraction patterns of 2-V_2O_5–ZrO_2 calcined at different temperatures for 1.5 h. ○, tetragonal phase ZrO_2; ●, monoclinic phase ZrO_2.

of pure ZrO_2. X-ray diffraction data indicated a tetragonal phase of ZrO_2 at 673 K, a two-phase mixture of the tetragonal and monoclinic ZrO_2 at 773 ~ 973 K, and a monoclinic phase of ZrO_2 at 1073 K. It is assumed that the interaction between vanadium oxide and ZrO_2 hinders the transition of ZrO_2 from amorphous to tetragonal phase (28). The presence of vanadium strongly influences the development of textural properties with temperature in comparison with pure ZrO_2. Moreover, for the samples of 5-V_2O_5/ZrO_2 and 9-V_2O_5/ZrO_2, the transition temperature from amorphous to tetragonal phase was higher by 150 and 200 K than that of pure ZrO_2, respectively. That is, the more the content of vanadium, the higher the transition temperature up to 9 mol%. For the samples above 9 mol%, however, the transition temperature did not increase more successively. These results are in agreement with those of DSC described later. As shown in Fig. 4, 5-V_2O_5/ZrO_2 was amorphous to X-ray diffraction up to 673 K, with a tetragonal phase of ZrO_2 at 773 K, a two-phase mixture of the tetragonal and monoclinic at 873–973 K, and a monoclinic phase at 1073 K. As shown in Fig. 5, 9-V_2O_5/ZrO_2 was amorphous to X-ray diffraction up to 773 K, with a tetragonal phase of ZrO_2 at 873 K and a monoclinic phase at 973–1073 K. No phases of vanadium oxide were observed up to 9 mol% at any calcination temperature, indicating a good dispersion of vanadium

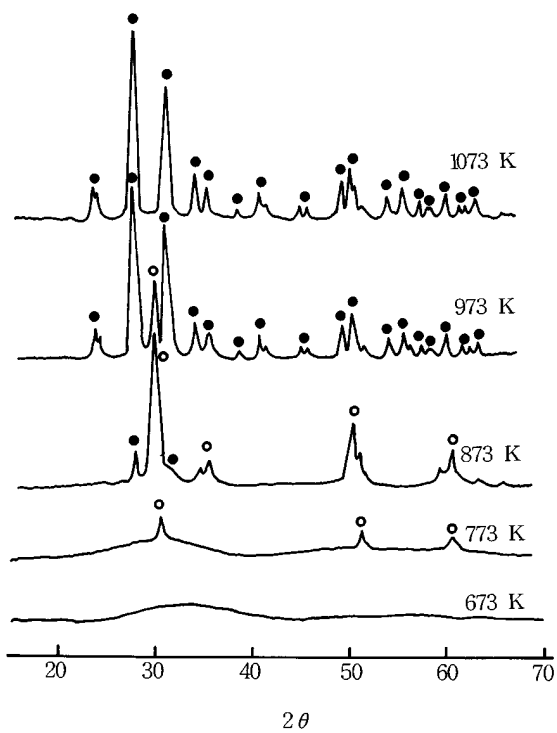

FIG. 4. X-ray diffraction patterns of 5-V_2O_5–ZrO_2 calcined at different temperatures for 1.5 h. ○, tetragonal phase ZrO_2; ●, monoclinic phase ZrO_2.

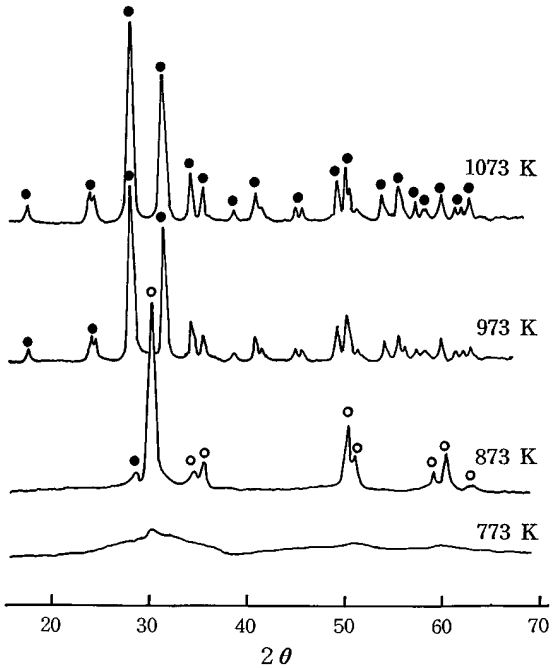

FIG. 5. X-ray diffraction patterns of 9-V_2O_5-ZrO_2 calcined at different temperatures for 1.5 h. ○, tetragonal phase ZrO_2; ●, monoclinic phase ZrO_2.

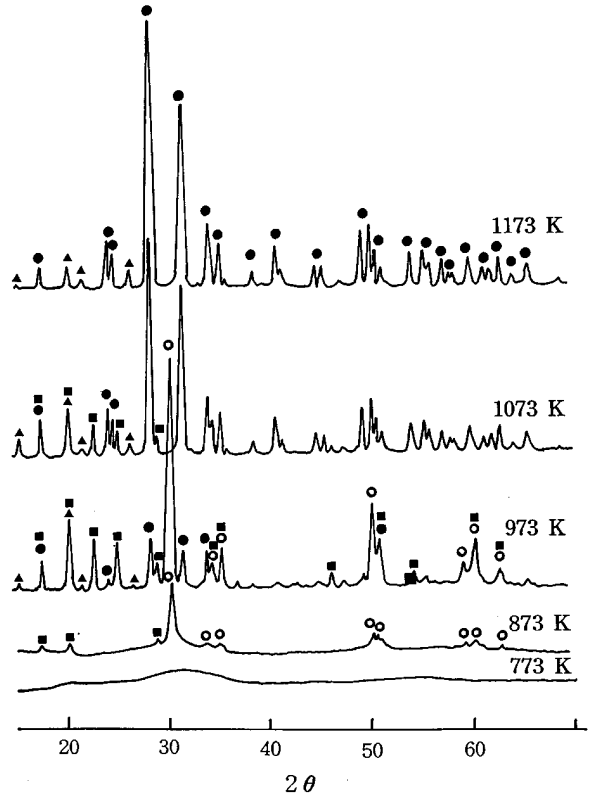

FIG. 6. X-ray diffraction patterns of 15-V_2O_5-ZrO_2 calcined at different temperatures for 1.5 h. ○, tetragonal phase ZrO_2; ●, monoclinic phase ZrO_2; △, orthorhombic phase V_2O_5; ■, cubic phase ZrV_2O_7.

oxide on the surface of the ZrO_2 support due to the interaction between them. These results are in good agreement with those of IR and ^{51}V NMR in Figs. 1 and 8.

As shown in Fig. 6, however, for 15-V_2O_5/ZrO_2 the cubic phase of ZrV_2O_7 was observed in the samples calcined at 873 K, and the diffraction pattern at 973 K may point to a coexisting crystalline V_2O_5 phase. At 1073 K of calcination temperature the peak intensities of ZrV_2O_7 decreased to some extent, resulting from thermal decomposition of the ZrV_2O_7 into zirconia and vanadia (36). Consequently, for sample calcined at 1173 K the ZrV_2O_7 phase disappeared due to the complete decomposition of ZrV_2O_7, leaving only the V_2O_5 phase and the monoclinic phase of ZrO_2. These results are in agreement with those of ^{51}V solid state NMR described later. In view of IR (Fig. 1) and NMR (Fig. 8), for high V_2O_5 loading samples, 15-V_2O_5/ZrO_2, and 20-V_2O_5/ZrO_2 calcined at 673 K, the crystalline of V_2O_5 is observed clearly. However, as shown in Fig. 6, the crystalline V_2O_5 on X-ray diffraction pattern is not found at 673 K of calcination temperature. This indicates that for samples calcined at 673 K the V_2O_5 crystallites formed are less than 4 nm in size, that is, beyond the detection capability of the XRD technique.

Thermal analysis

In X-ray diffraction pattern, it was shown that the structure of V_2O_5/ZrO_2 was different depending on the calcined temperature. To examine thethermal properties of precusors of samples more clearly, their thermal analysis was carried out and illustrated in Fig. 7. For pure ZrO_2, the DSC curve shows a broad endothermic peak below 453 K due to water elimination, and a sharp and endothermic peak at 702 K due to the ZrO_2 crystallization (37). In the case of V_2O_5/ZrO_2, two additional endothermic peaks appear at about 454 and 563 K due to the revolution of NH_3 and H_2O decomposed from NH_4VO_3. Also it is considered that an endothermic peak at 947 K is responsible for the melting of V_2O_5 and an exothermic peak around 989 K is due to the formation of ZrV_2O_7 crystalline described in X-ray diffraction patterns. However, it is of interest to see the influence of vanadium oxide on the crystallization of ZrO_2 from amorphous to tetragonal phase. As Fig. 7 shows, the exothermic peak due to the crystallization appears at 702 K for pure ZrO_2, while for V_2O_5/ZrO_2 samples it is shifted to higher temperatures. The shift increases with increasing vanadium oxide content up to 9 mol% of V_2O_5. Consequently, the exothermic peaks appear at 710.1 K for 1-V_2O_5/ZrO_2, 830.7 K for 5-V_2O_5/ZrO_2, and 874.6 K for 9-V_2O_5/ZrO_2.

For the samples above 9 mol% of V_2O_5, however, the shift of transition temperature did not occur more successively,

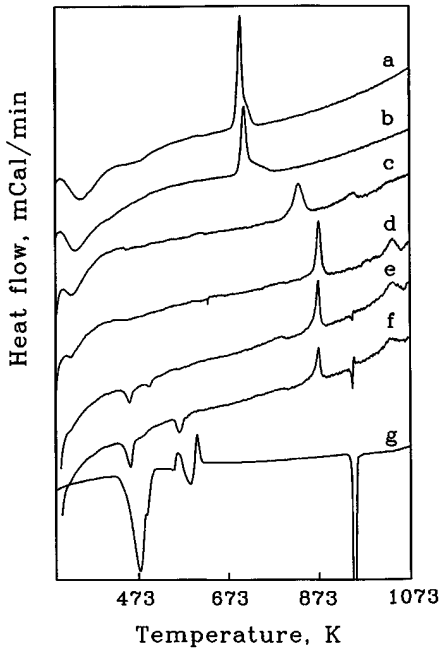

FIG. 7. DSC curves of precursors of catalysts: (a) ZrO_2, (b) 1-V_2O_5/ZrO_2, (c) 5-V_2O_5/ZrO_2, (d) 9-V_2O_5/ZrO_2, (e) 15-V_2O_5/ZrO_2, (f) 20-V_2O_5/ZrO_2, and (g) NH_4VO_3.

resulting in agreement with those of X-ray diffraction patterns described above. For the samples above 9 mol%, no further shift of transition temperature means that the content of vanadium oxide exceeding 9 mol% does not interact with the surface of zirconia. Moreover, as shown in Fig. 7, the results that the endothermic peaks at 947 K due to the melting of V_2O_5 are not observed for samples containing low content of V_2O_5 up to 9 mol% support the above discussion more absolutely. That is, it is clear that the interaction between V_2O_5 forming a monolayer on the surface of ZrO_2 and zirconia prevents V_2O_5 from melting and then only the amount of V_2O_5 exceeding 9 mol% melts easily.

On zirconia the V_2O_5 may be present as a monomolecular dispersion, covering most of the available surface (38). In view of results of IR, XRD, and DSC, it is concluded that the content of V_2O_5 forming a complete V_2O_5 monolayer on the surface of zirconia below the transition temperature of ZrO_2 is 9 mol%. It is relevant that the strong interaction between vanadium oxide and zirconia delays the transition of ZrO_2 from amorphous to tetragonal phase.

As shown in Fig. 10, the surface area of 9-V_2O_5/ZrO_2 is 150.0 m^2/g which is mainly contributed by ZrO_2, because V_2O_5 plays a role to protect the catalyst from sintering. So, we can calculate the area of one V_2O_5 molecule occupying the surface of ZrO_2 giving 2.3 molecules nm^{-2}. This result is very similar with 2.4 molecules nm^{-2} assumed by Hatayama *et al.* (12).

^{51}V Solid State NMR Spectra

Solid state NMR methods represent a novel and promising approach to vanadium oxide catalytic materials. The solid state ^{51}V NMR spectra of V_2O_5/ZrO_2 catalysts calcined at 673 K are shown in Fig. 8. There are three types of signals in the spectra of catalysts with varying intensities depending on V_2O_5 content. At the low loadings up to 9 mol% V_2O_5 a shoulder at about −300 ppm and the intense peak at −500∼650 ppm are observed. The former is assigned to the surface vanadium–oxygen structures surrounded by a distorted octahedron of oxygen atoms, while the latter is attributed to the tetrahedral vanadium–oxygen structures (39, 40).

However, the surface vanadium oxide structure is remarkably dependent on the metal oxide support material. Vanadium oxide on TiO_2 (anatase) displays the highest tendency to be six-coordinated at low surface coverages, while in the case of γ-Al_2O_3 a tetrahedral surface vanadium species is the favored (39). As shown in Fig. 8, at low vanadium loadings on ZrO_2 a tetrahedral vanadium species is exclusively dominant compared with an octahedral species. In general, it is known that low surface coverages favor a tetrahedral coordination of vanadium oxide, while at higher surface coverages vanadium oxide becomes increasingly octahedral-coordinated.

In order to calculate the relative amount of surface vanadium species the curve was analyzed by appropriate curve fitting as shown in Fig. 8. For 2-V_2O_5/ZrO_2 the amount of tetrahedral vanadium species was 86.5%, while that

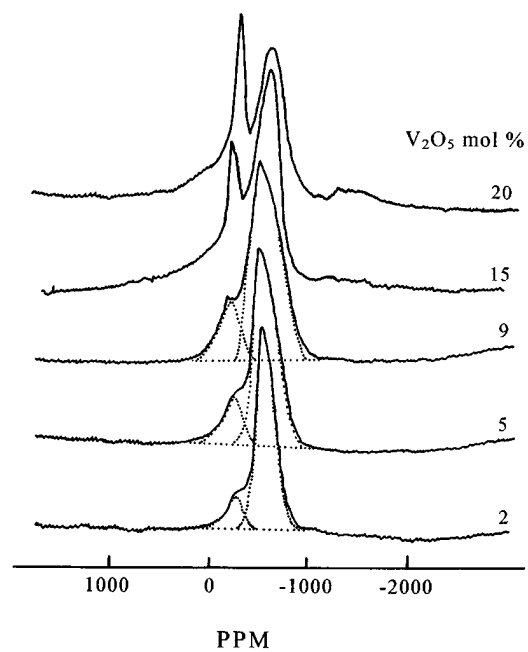

FIG. 8. Solid state ^{51}V NMR spectra of V_2O_5/ZrO_2 catalysts calcined at 673 K.

of octahedral species was estimated to be 13.5%. For 5-V_2O_5/ZrO_2 and 9-V_2O_5/ZrO_2 the percentage of octahedral species was estimated to be 17.6 and 21.7%, respectively. Namely, the relative amount of octahedral vanadium species increased with increasing vanadium loading. This finding agrees with earlier results of other workers (39, 40).

Increasing the V_2O_5 content on the ZrO_2 surface changes the shape of the spectrum to a rather intense and sharp peak at about −300 ppm and a broad low-intensity peak at about −1400 ppm, which are due to the crystalline V_2O_5 of square pyramid coordination (39). These observations of crystalline V_2O_5 for samples containing high V_2O_5 content above 9 mol% are in good agreement with the results of the IR spectra in Fig. 1. The spectra of 15-V_2O_5/ZrO_2 calcined at various temperatures are shown in Fig. 9. The shape of the spectrum is very different depending on the calcination temperature. For sample calcined at 673 K, a sharp peak at −300 ppm due to the crystalline V_2O_5 and an intense peak at −613 ppm attributable to V atoms in tetrahedral environment are observed. However, for sample calcined at 873 K, in addition to the above two peaks a sharp peak at −800 ppm due to crystalline ZrV_2O_7 appeared, indicating the formation of a new compound from V_2O_5 and ZrO_2 at high calcination temperature. As shown in Fig. 6, for samples calcined at 873–1073 K X-ray diffraction patterns of ZrV_2O_7 were observed. Roozeboom *et al.* reported the formation of ZrV_2O_7 from V_2O_5 and ZrO_2 at 873 K of calcination temperature (36, 38). At 1073 K of calcination temperature only a peak at −802 ppm due to the ZrV_2O_7 phase appeared, saying that most of V_2O_5 on the surface of ZrO_2 was consumed to form the ZrV_2O_7 compound. However, at 1173 K of calcination temperature we can observe only a sharp peak of crystalline V_2O_5 at −294 ppm, indicating the decomposition of ZrV_2O_7. These results are in good agreement with those of the X-ray diffraction patterns in Fig. 6. In the X-ray diffraction pattern of 15-V_2O_5/ZrO_2 calcined at 1173 K we can observe the presence of crystalline V_2O_5 and monoclinic ZrO_2 produced through the complete decomposition of ZrV_2O_7.

Surface Properties

It is necessary to examine the effect of vanadium oxide on the surface properties of catalysts, that is, specific surface area, acidity, and acid strength. The specific surface areas of samples calcined at 873 K for 1.5 h are plotted as a function of vanadium content in Fig. 10. The presence of vanadium oxide strongly influences the surface area in comparison with the pure ZrO_2. Specific surface areas of V_2O_5/ZrO_2 samples are much larger than that of pure ZrO_2 calcined at the same temperature, showing that surface area increases gradually with increasing vanadium content. It seems likely that the interaction between vanadium oxide and ZrO_2 protects catalysts from sintering. The dependence of the antisintering effect on vanadium oxide content is clear from Fig. 10. However, the surface areas for 5-V_2O_5/ZrO_2 and 9-V_2O_5/ZrO_2 are nearly the same, indicating that there is no correlation between surface area and V_2O_5 content at high coverage above 5 mol%.

The acid strength of the catalysts was examined by a color change method, using Hammett indicator (41) in dried benzene. Since it was very difficult to observe the color of indicators adsorbed on catalysts of high vanadium oxide content, a low percentage of vanadium content (0.1 mol%) was used in this experiment. The results are listed in Table 1. In this table, (+) indicates that the color of the base form

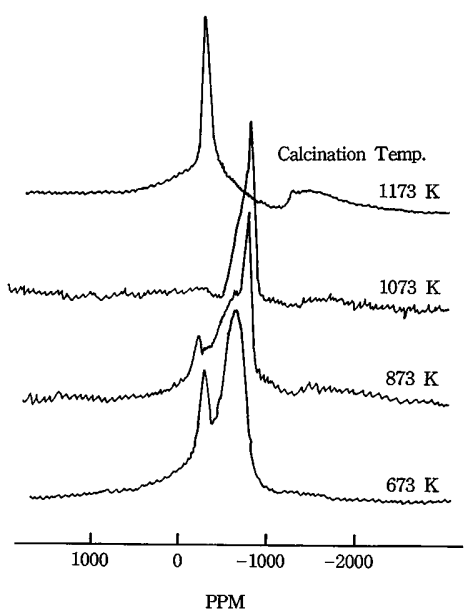

FIG. 9. Solid state ^{51}V NMR spectra of 15-V_2O_5/ZrO_2 catalysts calcined at different temperatures.

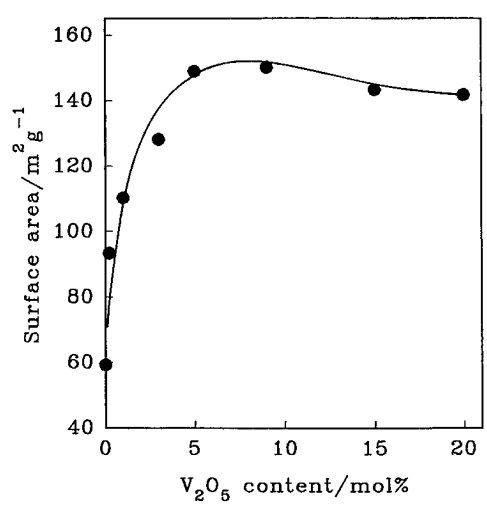

FIG. 10. Variation of surface area of V_2O_5/ZrO_2 calcined at 673 K with vanadium oxide content.

TABLE 1

Acid Strength of Catalysts

Hammett indicator	pK_a value of indicator	ZrO_2	0.1-V_2O_5/ZrO_2
Dimethylyellow	+3.3	+	+
Dicinnamalacetone	−3.0	+	+
Benzalacetophenone	−5.6	+	+
Anthraquinone	−8.2	−	+
P-Nitrotoluene	−11.35	−	+
Nitrobenzene	−12.4	−	−
2,4-Dinitrofluorobenzene	−14.5	−	−

was changed to that of the conjugated acid form. ZrO_2 evacuated at 673 K for 1 h has an acid strength Ho ≤ −5.6, while 0.1-V_2O_5/ZrO_2 was estimated to have a Ho≤−11.35, indicating the formation of new acid sites stronger than those of oxide components.

The acidity of catalysts, as determined by the amount of NH_3 irreversibly adsorbed at 503 K (30), is plotted as a function of the vanadium content in Fig. 11. Although pure ZrO_2 showed the acidity of 0.02 meq/g, 0.2-V_2O_5/ZrO_2 resulted in a remarkable increase in acidity (0.13 meq/g). As shown in Fig. 11, the acidity increases abruptly upon the addition of 0.2 mol% vanadium to ZrO_2, and then the acidity increases very gently with increasing vanadium oxide content reaching a maximum at 9-V_2O_5/ZrO_2. In view of Figs. 10 and 11, it is clear that the acidity runs parallel with the surface area, meaning that the values of acidity per surface area are nearly the same for all samples. Many combinations of two oxides have been reported to generate acid sites on the surface (42–44). The combination of ZrO_2 and V_2O_5 probably generates stronger acid sites and more acidity as compared with the separate components. A mechanism for the generation of acid sites by mixing two oxides has been proposed by Tanabe *et al.* (42). They suggest that the acidity generation is caused by an excess of a negative or positive charge in a model structure of a binary oxide related to the coordination number of a positive element and a negative element.

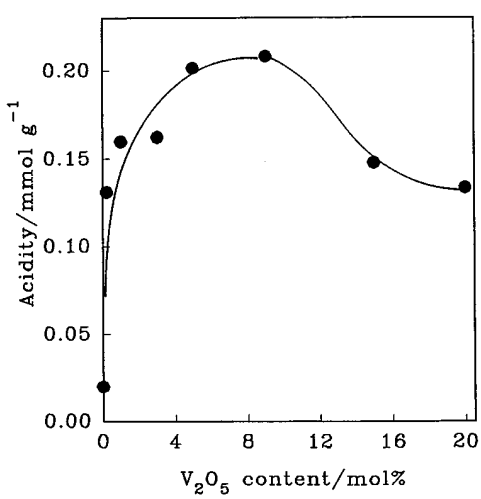

FIG. 11. Acidity of V_2O_5/ZrO_2 against vanadium oxide content.

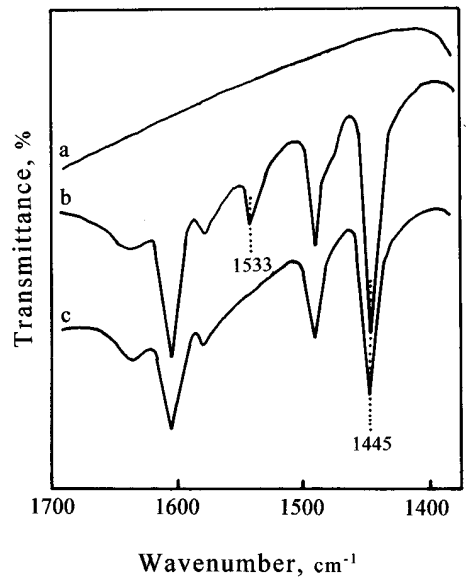

FIG. 12. Infrared spectra of pyridine adsorbed on 0.3-V_2O_5/ZrO_2: (a) background of 0.3-V_2O_5/ZrO_2, (b) pyridine adsorbed on 0.3-V_2O_5/ZrO_2, and (c) pyridine adsorbed on ZrO_2. Gas phase was evacuated at 250°C for 1 h after adsorption in (b) and (c).

Infrared spectroscopic studies of pyridine adsorbed on solid surfaces have made it possible to distinguish between Brønsted and Lewis acid sites (45). Figure 12 shows the IR spectra of pyridine adsorbed on 0.3-V_2O_5/ZrO_2 and ZrO_2 evacuated at 673 K for 1 h. For 0.3-V_2O_5/ZrO_2 the bands at 1533 are the characteristic peaks of pyridinium ion, which are formed on the Brønsted acid sites and the other set of adsorption peaks at 1445 cm^{-1} is contributed by pyridine coordinately bonded to Lewis acid sites (46), indicating the presence of both Brønsted and Lewis acid sites. Other samples having different vanadium content also showed the presence of both Lewis and Brønsted acids.

However, the only coordinated pyridine band at 1445 cm^{-1} is founded with ZrO_2. It is clear that the new Brønsted acid site which is not present on pure ZrO_2 is formed by the addition of V_2O_5 to ZrO_2. Miyata *et al.* reported that only Lewis acidity appears at low vanadium loading, while the catalyst after water treatment exhibits Brønsted acidity (16). The difference in our results and their results may be attributed to the different preparation method of the catalyst. They prepared vanadium–zirconia catalysts by a gas-phase method using $VOCl_3$ vapor, whereas we prepared them by the impregnation method using aqueous NH_4VO_3 solution.

CONCLUSIONS

This paper has shown that a combination of FTIR, DSC, NMR, and XRD can be used to perform the surface characterization of V_2O_5/ZrO_2 prepared by dry impregnation. The interaction between vanadium oxide and zirconia influences the physicochemical properties of prepared catalysts with calcination temperature. The presence of vanadium oxide delays the phase transitions of zirconia from amorphous to tetragonal in proportion to the vanadium oxide content up to 9 mol%. On the basis of results of DSC, XRD, and ^{51}V solid state NMR, the V_2O_5 content forming a complete monolayer on the surface of ZrO_2 was estimated to be 9 mol%, giving 2.3 V_2O_5 molecules/nm^2. Below the transition temperature of ZrO_2 from amorphous to tetragonal phase the ZrO_2 stabilizes supported vanadium oxide and vanadium oxide up to 9 mol% is well dispersed on the surface of ZrO_2. However, V_2O_5 loading exceeding the formation of complete monolayer (9 mol%) on the surface of ZrO_2 was well crystallized and observed in the spectra of IR and ^{51}V solid state NMR. Upon the addition of only a small amount of vanadium oxide (0.2 mol% V_2O_5) to ZrO_2, both the acidity and acid strength of the catalyst increases remarkably, showing the presence of two kinds of Brønsted and Lewis acid sites on the surface of V_2O_5/ZrO_2.

ACKNOWLEDGMENT

This paper was supported by the Research Program of Kyungpook National University and partly supported by the Research Center for Catalytic Technology.

REFERENCES

1. Wainwright, M. S., and Foster, N. R., *Catal. Rev.* **19**, 211 (1979).
2. Dadyburjor, D. B., Jewur, S. S., and Ruckenctein, E., *Catal. Rev.* **19**, 293 (1979).
3. Nakagawa, Y., Ono, T., Miyata, H., and Kubokawa, Y. J., *Chem. Soc. Faraday Trans. 1.* **79**, 2929 (1983).
4. Miyata, H., Kohno, M., Ono, T., Ohno, T., and Hatayama, F. J., *Chem. Soc. Faraday Trans. 1.* **85**, 3663 (1989).
5. Gellings, P. J., *in* "Spec. Per. Rep. Catalysis" (G. C. Bond and G. Webb, Eds.), Vol. 7, p. 105. Royal Society of Chemistry, London, 1985.
6. Bosch, H., and Janssen, F., *Catal. Today* **2**, 369 (1988).
7. Forzatti, P., Tronoconi, E., Busca, G., and Titarellp, P., *Catal. Today* **1**, 209 (1987).
8. Busca, G., Elmi, A. S., and Forzatti, P., *J. Phys. Chem.* **91**, 5263 (1987).
9. Elmi, A. S., Tronoconi, E., Cristiani, C., Martin, J. P. G., and Forzatti, P., *Ind. Eng. Chem. Res.* **28**, 387 (1989).
10. Miyata, H., Fujii, K., Ono, T., Kubokawa, Y., Ohno, T., and Hatayama., F., *J. Chem. Soc. Faraday Trans. 1* **83**, 675 (1987).
11. Cavani, F., Centi, G., Foresti, E., and Trifiro, F., *J. Chem. Soc. Faraday Trans. 1* **84**, 237 (1988).
12. Hatayama, F., Ohno, T., Maruoka, T., and Miyata, H., *J. Chem. Soc. Faraday Trans.* **87**, 2629 (1991).
13. Arco, M. del, Holgado, M. J., Martin, C., and Rives, V., *Langmiur* **6**, 801 (1990).
14. Centi, G., Pinelli, D., Trifiro, F., Ghoussoub, D., Guelton, M., and Gengembre, L., *J. Catal.* **130**, 238 (1991).
15. Inomata, M., Mori, K., Miyamota, A., and Murakami, Y., *J. Phys. Chem.* **87**, 761 (1983).
16. Miyata, H., Kohno, M., Ono, T., Ohno, T. and Hatayama, F., *J. Mol. Catal.* **63**, 181 (1990).
17. Scharf, U., Schraml-Marth, M., Wokaun, A., and Baiker, A., *J. Chem. Soc. Faraday Trans.* **87**, 3299 (1991).
18. Miyata, H., Kohno, M., Ono, T., Ohno, T., and Hatayama, F., *J. Mol. Catal.* **63**, 181 (1990).
19. He, M. Y., and Ekerdt, J. G., *J. Catal.* **90**, 17 (1984).
20. Maehashi, T., Maruya, K., Domen, K., Aika, K., and Onishi, T., *Chem. Lett.* 747 (1984).
21. Yamaguchi, T., Sasaki, H., and Tanabe, K., *Chem. Lett.* 1017 (1973).
22. Davis, B. H., and Ganesan, P., *Ind. Eng. Chem. Prod. Res. Dev.* **18**, 191 (1979).
23. Iizuka, T., Tanaka, Y., and Tanabe, K., *J. Catal.* **76**, 1 (1982).
24. Turlier, P., Dalmon, J. A., and Martin, G. A., *Stud. Surf. Sci. Catal.* **11**, 203 (1982).
25. Szymanski, R., Charcosset, H., Gallezot, P., Massardier, J., and Tournayan, L., *J. Catal.* **97**, 366 (1986).
26. Sohn, J. R., and Kim, H. J., *J. Catal.* **101**, 428 (1986).
27. Sohn, J. R., and Kim, H. W., *J. Mol. Catal.* **52**, 361 (1989).
28. Sohn, J. R., and Ryu, S. G., *Langmuir* **9**, 126 (1993).
29. Hayashi, S., and Hayamizu, K., *Bull. Chem. Soc. Jpn.* **63**, 961 (1990).
30. Sohn, J. R., and Ozaki, A., *J. Catal.* **61**, 29 (1980).
31. Sohn, J. R., and Jang, H. J., *J. Mol. Catal.* **64**, 349 (1991).
32. Mori, K., Miyamoto, A., and Murakami, Y., *J. Chem. Soc. Faraday Trans.* **83**, 3303 (1987).
33. Bjorklund, R. B., Odenbrand, C. U. I., Brandin, J. G. M., Andersson, L. A. H., and Liedberg, B., *J. Catal.* **119**, 187 (1989).
34. Torralvo, M. J., Alario, M. A., and Soria, J., *J. Catal.* **86**, 473 (1984).
35. Clearfield, A., *Inorg. Chem.* **3**, 146 (1964).
36. Roozeboom, F., Mittelmeljer-Hazeleger, M. C., Moulijn, J. A., Medema, J., de Beer, V. H. J., and Gellings, P. J., *J. Phys. Chem.* **84**, 2783 (1980).
37. Livage, J., Doi, K., and Mazieres, C., *J. Am. Ceram. Soc.* **51**, 349 (1968).
38. Roozeboom, F., Fransen, T., Mars, D., and Gellings, P. J. Z., *Anorg. Allg. Chem.* **449**, 25 (1979).
39. Eckert, H., and Wachs, I. E. J., *Phys. Chem.* **93**, 6796 (1989).
40. Reddy, B. M., Reddy, E. P., Srinivas, S. T., Mastikhim, V. M., Nosov, N. V., and Lapina, O. B., *J. Phys. Chem.* **96**, 7076 (1992).
41. Hammett, L. P., and Deyrup, A. J., *J. Am. Chem. Soc.* **54**, 2721 (1932).
42. Itoh, M., Hattori, H., and Tanabe, T., *J. Catal.* **35**, 225 (1974).
43. Dzisko, V. A., *in* "Proceedings, 3rd International Congress on Catalysis, Amsterdam, 1964." Vol. 1, No. 19. Wiley, New York, 1965.
44. Miura, M., Kubota, Y., Iwaka, T., Takimoto, K., and Muraoka, Y., *Bull. Chem. Soc. Jpn.* **42**, 1476 (1969).
45. Parry, E. P., *J. Catal.* **2**, 371 (1963).
46. Connell, G., and Dumesic, J. A., *J. Catal.* **105**, 285 (1987).